Active Spin Stabilization for an Autonomous Spacecraft

Vítor Emanuel Andrade Narciso
vitor.narciso@tecnico.ulisboa.pt

Instituto Superior Técnico, Lisboa, Portugal

October 2022

Abstract

Single-spin passive attitude stabilization is a simple method of maintaining the spacecraft pointing in a certain direction and reduce power consumption, as a rigid body spinning about its principal major axis of inertia is in a stable rotation condition. According to linear algebra, there always exists a body reference frame where the inertia matrix is diagonal, which guarantees that the axes associated with the largest and smallest values of the diagonal correspond to the principal major and minor axes of inertia, respectively. However, the initial estimate of the principal moments of inertia and respective reference frame can be incorrect as they are notoriously difficult to determine. This manuscript addresses the problem of designing an active spin stabilization system, through the development of two GNC solutions that stabilize the spin motion of the vehicle about the principal major axis of inertia, even when it is uncertain. In the first approach, an extended Kalman filter is designed to estimate the rotation between the body-fixed frame and the principal axes of inertia, allowing then to provide the properly aligned angular velocity vector as a reference to the controller. As an alternative, a nonlinear control law is implemented to correct the spinning direction reference towards a principal axis avoiding the computational complexity of the filter. These GNC algorithms include an angular velocity controller to track the desired reference, with global asymptotic stability for a constant reference. The proposed solutions are extensively tested in Monte Carlo simulations, resulting in propellant savings over 96%.
Keywords: Spin Stabilization, Satellite, Navigation Filter, Extended Kalman Filter, PI Controller

1. Introduction

1.1. Motivation and Goals

Guidance, Navigation and Control (GNC) systems are a continuous object of study in the scientific community, as well as in the space industry. Despite this, and given the conservative nature of the industry, many of the tools used are already classic and out of date with the state of the art both in terms of control theory and estimation systems, as well as current computing capabilities. For this reason, there are still huge engineering challenges associated with these two fundamental systems [1].

Spin stabilization is a method used to maintain the pointing direction of a spacecraft, while rotating around its own pointing axis. This is achieved using the gyroscopic effect - a principle that states a rigid body spinning about its major or minor axis of inertia is in a stable rotation condition, i.e., it will keep the direction of its spinning axis fixed with respect to the inertial space reference frame, even in the presence of small disturbances [2].

The main concern when tackling spin stabilized satellites is to ensure that the passive scheme method does not incur additional energy costs - it is indeed passive. To accomplish so, the spacecraft must be rotating around its major or minor axis of inertia, in order to guarantee stability and avoid fuel consumption to thrust and keep the satellite spinning around a non-stable axis. According to linear algebra, there always exists a body reference frame where the inertia matrix is diagonal, which guarantees that the axes associated with the largest and smallest values of the diagonal correspond to the principal major and minor axes of inertia, respectively.

However, the initial estimate of the principal axes of inertia and respective reference frame can be incorrect as they are notoriously difficult to determine and, as time passes, the satellite may change its mass and/or geometry, for instance opening solar panels or consuming fuel, causing the appearance of products of inertia.

In summary, this work addresses the problem of designing an active spin stabilization system, i.e., a GNC solution that provides the proper angular velocity vector as a reference to the controller, which is necessary to rotate the spacecraft and align its spin axis with the principal major axis of inertia. The main goal can be broken down into the following objectives: 1) Study and review the most relevant topics regarding spacecraft attitude determination and control for a satellite in spin stabilization; 2) Design and implement an active spin stabilization method applied to a Spacecraft Plant model in a realistic space environment; 3) Analyze and compare the results obtained from different algorithms in simulation tests, to draw conclusions and determine future improvements.

1.2. State of the Art

Attitude estimation and control is a problem with an extensive historical background that continues to attract intensive research, and several techniques to solve the inertia matrix estimation problem regarding spin stabilized satellites have been proposed in the literature. Authors such as J. R. Wertz, M.J. Sidi, Y. Yang, F. L. Markley, and J. L. Crassidis have published many articles and books exploring this subject [1, 2, 3, 4], which will be taken into account during the Theoretical Background in Section 2.

The first satellites, such as the Sputnik in 1957, did not have an ADCS, or relied on passive stabilization methods, while control torques were computed on the ground and transmitted to the spacecraft [1]. Some of the earliest proposals to address this problem were provided by algebraic solutions based on real-time measurements, such as the Triaxial Attitude Determination (TRIAD), the Davenport's q-method and the Quaternion Estimator (QUEST) algorithms. Most recent solutions try to find the best estimate of the true attitude using dynamical models and measurements, i.e., they retain information from a series of measurements taken over time. These type of approaches are called recursive attitude determination methods. One of the most popular recursive algorithms is the Kalman Filter (KF), originally developed in 1961 as a tool for linear estimation [5].

For the last years, the Extended Kalman Filter (EKF) has been the prime choice in ADCS designs for CubeSats, becoming the most used method for spacecraft attitude determination. However, this filters do not guarantee optimality, stability or convergence, and to overcome the poor performance or even divergence arising from the linearization implicit in the EKF, other nonlinear attitude estimation methods have been arising. Some recent alternatives are the Unscented Filter (UF), the two-step optimal estimator, and nonlinear observers [5].

While spacecraft attitude estimation development history is well documented, attitude control methods past is known to a lesser extent. Robert Roberson [6] claims that the first published works regarding spacecraft attitude control appeared during the mid 1950s. At the time, spacecraft used passive control methods, i.e., spin and gravity-gradient stabilization or a momentum wheel [1]. As pointing requirements became more demanding and on-board computers have become more capable, spacecraft Attitude Control System (ACS) designs have shifted towards active control methods, namely three-axis stabilization. The most common in spacecraft attitude control are the Proportional-Integral-Derivative (PID) controller and the Linear Quadratic Regulator (LQR) algorithm.

Nowadays, still about 95% of aerospace industrial applications continue to be operated by PID controllers, just as they were back in the 1960s period. However, due to the digital revolution and exponential growth in computational power during the last years, modern control designs have been developed and adapted for the space industry to deal with the increasing parametric and non-parametric uncertainty present in the complex space missions underdevelopment. These fault-tolerant controller designs include the so-called Robust Control methods, Sliding Mode Control (SMC) and Model Predictive Control (MPC).

Although presently the space industry relies more on the development of active stabilization schemes, one problem that still remains contemporary for passive stabilization schemes is the inertia matrix estimation. The term "moment of inertia" was introduced in 1765 by Leonhard Euler [7], and incorporated into Euler's second law. In the aerospace industry, moment of inertia theory was applied for the first time by William Hale, when the concept of spin stabilization was invented in the middle of the 19th century. According to the literature, in-flight estimates of the inertia tensor have been researched since 2002, resorting to a least squares minimization problem [8]. Later, the constrained least squares [9] and EKF-based methods [10] were applied for inertia matrix estimation. More recently, bolder approaches have emerged such as the implementation of an Unscented Kalman Filter (UKF) to process the light-curve and angles from on-board astronomic photographies and estimate orientation, position, velocity and inertia parameters [11], or even the design of a semi-adaptive filter based on the linear regression model, to achieve low variance estimates [12].

2. Theoretical Background

2.1. Attitude Representations

Spacecraft attitude can be defined as its orientation in space with respect to a specific reference frame. There are various forms to represent this orientation, including matrices and three-component vectors, and these formalisms are known as attitude representations or parameterizations. The most representative forms of attitude representation are the Direction Cosine Matrix (DCM), the Euler Angles, the Quaternions, and the Axis-Angle, which are discussed in this document based on references from J. L. Crassidis and Y. Yang [1, 4].

1) Direction Cosine Matrix (DCM): The most general form of attitude representation is the DCM, a rotation matrix that belongs to the special orthogonal group defined as $SO(3) := \{\boldsymbol{A} \in \mathbb{R}^{3\times3} : \det(\boldsymbol{A}) = 1 \wedge \boldsymbol{A}\boldsymbol{A}^T = \boldsymbol{A}^T\boldsymbol{A} = \boldsymbol{I}$. An arbitrary vector $\boldsymbol{r} \in \mathbb{R}^3$ can be rotated from one frame to another using a DCM. For example, the relative orientation of the spacecraft body frame $\mathcal{B}$ w.r.t. the inertial reference frame $\mathcal{I}$ is provided by a 3×3 matrix, obtained from the inner product of the basis unit vectors, i.e.,

$$\boldsymbol{A}_{\mathcal{BI}} = \begin{bmatrix} b_1 \cdot i_1 & b_1 \cdot i_2 & b_1 \cdot i_3 \\ b_2 \cdot i_1 & b_2 \cdot i_2 & b_2 \cdot i_3 \\ b_3 \cdot i_1 & b_3 \cdot i_2 & b_3 \cdot i_3 \end{bmatrix} \tag{1}$$

2) Euler Angles: The most common way of representing a rigid body attitude is a set of three successive rotations about the x, y and z axes, defined according to the respective Euler angles (ϕ, θ and ψ). To transform an Euler angles vector ($[\phi, \theta, \psi]^T$) in its corresponding rotation matrix ($\boldsymbol{R}_{ijk} : \mathbb{R}^3 \longrightarrow SO(3)$, for $i, j, k \in \{1, 2, 3\}$), the expression required is the product of the coordinate matrices representing each individual rotation, as given by

$$\boldsymbol{R}_{ijk}(\phi, \theta, \psi) = \boldsymbol{R}_i(\phi)\boldsymbol{R}_j(\theta)\boldsymbol{R}_k(\psi) \tag{2}$$

The Euler angles representation and its function depend vastly on the rotation sequence, that is, the coordinate rotations order. As it is the most commonly used for aerospace engineering applications, the rotation matrices sequence chosen is the asymmetric set $(1, 2, 3)$, whose attitude matrix results in

$$\boldsymbol{R}_{123}(\phi, \theta, \psi) = \begin{bmatrix} c_\theta c_\psi & c_\theta s_\psi & -s_\theta \\ s_\phi s_\theta c_\psi - c_\phi s_\psi & s_\phi s_\theta s_\psi + c_\phi c_\psi & s_\phi c_\theta \\ c_\phi s_\theta c_\psi + s_\phi s_\psi & c_\phi s_\theta s_\psi - s_\phi c_\psi & c_\phi c_\theta \end{bmatrix} \tag{3}$$

3) Unit Quaternions: Unlike the Euler angles, a quaternion represents attitude as a rotation according to a rotational angle $\alpha \in \mathbb{R}$ around a rotational axis $\hat{\boldsymbol{e}} \in \mathbb{R}^3$. In fact, according to the *Euler's rotation theorem*, any displacement of a rigid body such that a point on the rigid body remains fixed, is equivalent to a single rotation about some axis that runs through the fixed point. Therefore, any rotation in three dimensions can be represented as a combination of a scalar α and an unit vector $\hat{\boldsymbol{e}}$.

Hereinafter, a quaternion $\boldsymbol{q} \in \mathbb{H}$ will be considered a four-component vector with a three-vector part $\boldsymbol{q_v}$ and a scalar part q_4:

$$\boldsymbol{q} = \begin{bmatrix} q_1 & q_2 & q_3 & q_4 \end{bmatrix}^T = \begin{bmatrix} \boldsymbol{q_v} \\ q_4 \end{bmatrix} \tag{4}$$

This definition is conceptually different from the one first introduced by Hamilton, resulting in distinct properties and operations used throughout this document. In conformance with this notation, and as usual in space applications, a normalized quaternion may be defined as

$$\boldsymbol{q}(\hat{\boldsymbol{e}}, \alpha) = \begin{bmatrix} \hat{\boldsymbol{e}} \sin(\alpha/2) \\ \cos(\alpha/2) \end{bmatrix} \tag{5}$$

The quaternion multiplication can also be used to prove that the product of two quaternions representing two consecutive rotations, can be summed up in a single rotation. Attitude kinematics in quaternions is represented using the matrix expression for the quaternion product. Considering $\boldsymbol{\omega} \in \mathbb{R}^3$ as the angular velocity in the spacecraft body frame and $\dot{\boldsymbol{q}}$ as the quaternion derivative, the relation is described as

$$\dot{\boldsymbol{q}} = \frac{1}{2}\boldsymbol{Q}(\boldsymbol{q}) \begin{bmatrix} 0 \\ \boldsymbol{\omega} \end{bmatrix} = \frac{1}{2}\boldsymbol{\Omega}(\boldsymbol{\omega})\boldsymbol{q} \tag{6}$$

where $\boldsymbol{\Omega}(\boldsymbol{\omega}) \in \mathbb{R}^{4\times4}$ is the dynamics matrix, defined as

$$\boldsymbol{\Omega}(\boldsymbol{\omega}) \equiv \begin{bmatrix} -[\boldsymbol{\omega}\times] & \boldsymbol{\omega} \\ -\boldsymbol{\omega}^T & 0 \end{bmatrix} \tag{7}$$

4) Axis-Angle: In mathematics, the axis-angle representation defines a three-dimensional rotation about a fixed axis, specified by a unit vector $\hat{\boldsymbol{e}}$, according to a rotation angle α, and is a convenient parameterization when dealing with rigid body dynamics. As stated before, this two-parameter convention is valid to represent any rotation, in agreement with *Euler's rotation theorem*.

An attitude matrix $\boldsymbol{A}$, conforming to the $SO(3)$ definition and to the axis-angle representation, can be provided to express the relation between two vectors as

$$\boldsymbol{A}(\hat{\boldsymbol{e}}, \alpha) = (\cos(\alpha))\boldsymbol{I}_3 + \sin(\alpha)[\hat{\boldsymbol{e}}\times] + (1 - \cos(\alpha))\hat{\boldsymbol{e}}\hat{\boldsymbol{e}}^T \tag{8}$$

where $[\hat{\boldsymbol{e}}\times]$ is the skew-symmetric cross product matrix formed from vector $\hat{\boldsymbol{e}}$. Alternatively, as presented in equation (5), the axis-angle parameters can also be handled as variables to define the normalized quaternion.

2.2. Reference Frames

In physics and astronomy, a reference frame is a coordinate system specified by its origin and the orientation of its coordinate axes. Two of the most frequently used reference frames are Earth Centered Inertial (ECI) and Spacecraft Body Frame [1, 4, 13].

To study the attitude of a spacecraft orbiting the Earth, the ECI frame is the go-to coordinate system. It has its origin at the center of mass of the Earth and three orthogonal axes fixed relative to it. The Z-axis is aligned with the mean North Pole, the X-axis points to the Vernal Equinox direction, and the Y-axis completes the right-handed system. Although the ECI has a linear acceleration due to Earth's translation movement around the Sun, that effect may be neglected for attitude analysis and it can be considered inertial with respect to the stars. Hence, these coordinates are used to define the *inertial reference frame*.

The spacecraft body frame has its origin at the center of mass of the satellite and is vehicle-carried, i.e., its axes rotate with the spacecraft and are usually fixed to the principal axes of inertia (14). In this reference frame, which is denoted by $\mathcal{B} = \{b_1, b_2, b_3\}$, the Z_b-axis is determined according to the major principal axis of inertia direction, the Y_b-axis is aligned with the minor principal axis of inertia, and the X_b-axis points to the intermediate principal axis of inertia, complying with the right-hand rule.

However, this thesis introduces a nuance to the body reference frame $\mathcal{B}$. In reality, it is slightly rotated w.r.t. the principal axes of inertia, as a means to reproduce the misalignment caused by an initial computation error. Even so, all equations use this unaligned reference frame when referring to the body coordinate system to prevent any ambiguity. On the other hand, the principal axes of inertia now constitute a body-centered reference frame denoted by $\mathcal{J} = \{j_1, j_2, j_3\}$. In Section 4, a representation of both coordinate systems can be seen in Figure 1.

2.3. Attitude Kinematics and Dynamics

Rigid body dynamics studies the movement of systems under the action of external forces, and are described by the laws of kinematics. The distinction between kinematics and dynamics is that the former covers aspects of motion that can be analyzed without consideration of forces or torques. When those are introduced, it enters the realm of dynamics [1].

Attitude kinematics analyzes how the orientation of the spacecraft changes in time according to the angular velocity, $\boldsymbol{\omega} \in \mathbb{R}^3$. As defined in equation (6), the nonlinear spacecraft kinematics equations of motion can be represented in terms of unit quaternions. A significant advantage of the quaternion parameterization is that the kinematic equation becomes linear, hence it is the attitude kinematics representation implemented in this document.

Euler's second law of motion [14] states $\dot{\boldsymbol{h}} + \boldsymbol{\omega} \times \boldsymbol{h} = \boldsymbol{\tau}$, where $\boldsymbol{h} \in \mathbb{R}^3$ is the spacecraft's angular momentum about its center of mass, $\dot{\boldsymbol{h}} \in \mathbb{R}^3$ is its respective time derivative, and $\boldsymbol{\tau} \in \mathbb{R}^3$ is the total torque acting on the body about its center of mass. The angular momentum vector $\boldsymbol{h}$ is given by $\boldsymbol{h} = \boldsymbol{J}\boldsymbol{\omega_I}$, with $\boldsymbol{\omega_I} = [\omega_{I1}, \omega_{I2}, \omega_{I3}]^T$ being the angular velocity vector of the spacecraft body frame w.r.t. the inertial frame and expressed in the body frame, and $\boldsymbol{J} \in \mathbb{R}^{3\times3}$ being the moment of *inertia tensor* or *inertia matrix* of a spacecraft [4]. Then, assuming a constant inertia tensor in the body frame $\mathcal{B}$, Euler's second law of motion can be rewritten as

$$\boldsymbol{J}\dot{\boldsymbol{\omega}}_{\boldsymbol{I}} = -\boldsymbol{\omega}_{\boldsymbol{I}} \times \boldsymbol{J}\boldsymbol{\omega}_{\boldsymbol{I}} + \boldsymbol{\tau} \tag{9}$$

At last, it should be recognized that the external torque $\boldsymbol{\tau}$ is composed of two parts - the control torque $\boldsymbol{\tau}_u \in \mathbb{R}^3$, that is, the input commanded by the Control System, and the disturbances torque $\boldsymbol{\tau}_d \in \mathbb{R}^3$, which represents the torques acting on a spacecraft subject to the surrounding environment. Thus, the dynamics equation (9) can be extended to

$$\boldsymbol{J}\dot{\boldsymbol{\omega}}_{\boldsymbol{I}} + \boldsymbol{\omega}_{\boldsymbol{I}} \times \boldsymbol{J}\boldsymbol{\omega}_{\boldsymbol{I}} = \boldsymbol{\tau}_u + \boldsymbol{\tau}_d \tag{10}$$

In space, there are no large torques applied to the satellites, and hence minor influences integrated over time play major roles in governing the attitude dynamics of spacecraft. External torques arise from the interaction of a space vehicle with its environment and require a specification of both vehicle properties and spacial environment to be calculated. All disturbance torques are induced by external forces acting outside the center of mass (CM). The most representative perturbation torques are the gravity-gradient torque, the solar radiation pressure torque, the magnetic torque and the aerodynamic torque.

Gravitational torques are fundamental to the attitude dynamics of spacecraft and are the most important external disturbances, exceeding the magnitude of the next-largest perturbation by up to six times. From Newton's law of universal gravitation and following the previous assumptions, the gravity-gradient disturbance torque $\boldsymbol{\tau}_{gg} \in \mathbb{R}^3$ can be defined as

$$\boldsymbol{\tau}_{gg} = \frac{3\mu_E}{r_c^5}\boldsymbol{r}_c \times \boldsymbol{J}\boldsymbol{r}_c \tag{11}$$

where μ_E is the Earth gravitational parameter, $r_c = ||\boldsymbol{r}_c||$ is the orbit radius norm (i.e., the distance from Earth's center of mass to the satellite), $\boldsymbol{r}_c$ is the orbit radius vector expressed in the spacecraft body frame, and $\boldsymbol{J}$ is the satellite's inertia matrix [4, 13].

2.4. Sensors and Actuators

To determine and control a spacecraft's orientation, attitude hardware components must be installed in the satellite. For attitude determination, there needs to be measurement equipment to ascertain the orientation or at least provide measurements to be used for attitude estimation - these are called sensors. On the other hand, actuators are the components responsible for producing the control torques necessary to achieve the desired attitude [3, 4].

During the last decades, attitude sensor development has led to increased resolution and accuracy, in addition to a decrease in size, weight, and power requirements. Thus, most sensors have been adapted for small satellite applications, as its the case for sun sensors, magnetometers, star trackers, and gyroscopes [1].

In this study, the sensor considered for the satellite is a gyroscope (or *gyro* for short), a device that can measure the angular velocity with very low noise interference. The measurements can be numerically integrated by an onboard computer to provide an estimate for the attitude, or even directly used in attitude control. These rate sensors are constituted by a rotor that rotates around its spin axis and maintains its spin direction, regardless of the outer frame orientation and opposing any attempts to change its attitude, specifically, exhibiting precession and/or nutation motions. One of the principal drawbacks regarding gyroscopes is that they hold an inherent bias that results in a constant drift. Nonetheless, gyroscopes are still useful for this application, as they provides direct angular velocity measurements for attitude determination.

On the other hand, actuator technologies have also been scaled down over time to be appropriate for microsatellites and cubesats. These equipments can be divided into two separate classes - momentum exchange devices, that generate torques that can be considered internal, and reaction-type actuators, that generate torques that can be considered external to the spacecraft. The most commonly used momentum actuators are reaction wheels (RWs) and control moment gyros (CMGs), while the most widely implemented reaction actuators are magnetic torque rods and thrusters. Some of them, such as RWs and thrusters, can easily provide the desired torques, but magnetic torque rods and CMGs may require alternative methods to reach the intended control input [4].

Thrusters are spacecraft propulsion devices that use propellants to generate both forces and torques, so they can be used for trajectory and attitude control. The force $\boldsymbol{f}_{prop} \in \mathbb{R}^3$ and torque $\boldsymbol{\tau}_{prop} \in \mathbb{R}^3$ provided by a thruster are defined as

$$\boldsymbol{f}_{prop} = -\dot{m}\boldsymbol{v}_m \tag{12}$$

$$\boldsymbol{\tau}_{prop} = \boldsymbol{r} \times \boldsymbol{f}_{prop} \tag{13}$$

where $\dot{m}$ is the expelled mass flow rate, $\boldsymbol{v}_m$ is the expelled mass velocity relative to the spacecraft, and $\boldsymbol{r}$ is the moment arm vector from the center of mass to the thruster. There are three types of thrusters that are commonly used for attitude control - cold gas, monopropellant and electric thrusters, and they are frequently used to complement the main ACS actuators, as they are more suitable to be implemented as a correction actuator due to the budget limit related to fuel consumption. Therefore, as the scope of this work consists in correcting the alignment between the satellite's spin-axis and its principal major axis of inertia, it constitutes a common secondary application, thus, an energy-efficient actuator like the thrusters can be used to effectively reach the desired goal.

3. Passive Spin Stabilization

Almost all spacecraft employ the spin stabilization effect during part or all of their lifetime in space. Many satellites are spin stabilized to take advantage of the gyroscopic effect and, hence, maintain their spinning axis stable and avoid unnecessary power consumption. The dynamic attributes of spinning bodies are used to stabilize satellites' attitude within both the orbital maneuvering stage and the final mission orbit. However, it is important to notice that only a body spinning about its major or minor axes of inertia will keep the direction of its spin axis fixed with respect to the inertial space. In this regard, an overview of the principal axes of inertia, rotation matrices and the conditions for spin stability about any principal axis in the absence of external torques are studied in this section.

3.1. Principal Axes of Inertia

The inertia matrix $\boldsymbol{J}$ is composed of diagonal elements or *moments of inertia*, and non-diagonal elements or *products of inertia*. In case the inertia tensor is diagonal, then the inertia matrix is considered to be defined according to the *principal axes of inertia* ($\boldsymbol{X}_b$, $\boldsymbol{Y}_b$, $\boldsymbol{Z}_b$). Hence, the larger and smaller values of the diagonal correspond to the spin-stable major and minor axis of inertia, respectively [2].

The problem at hand is to determine the orientation of the principal axes of inertia and adopt them as the spacecraft body frame. Thus, to define a new reference frame in which the inertia tensor is diagonal, an axis rotation must be performed. For this case, the eigendecomposition into the product of a rotation matrix $\boldsymbol{R} \in SO(3)$ and a diagonal matrix $\boldsymbol{\Lambda} \in SO(3)$ is given by

$$\boldsymbol{J} = \boldsymbol{R}\boldsymbol{\Lambda}\boldsymbol{R}^T \quad \text{with} \quad \boldsymbol{\Lambda} = \begin{bmatrix} J_x & 0 & 0 \\ 0 & J_y & 0 \\ 0 & 0 & J_z \end{bmatrix} \tag{14}$$

The columns of the rotation matrix $\boldsymbol{R}$ are the inertia matrix eigenvectors and define the directions of the principal axes of inertia in the body frame, while the constants J_x, J_y and J_z are called the *principal moments of inertia* and are the inertia tensor eigenvalues. This result is a form of Sylvester's law of inertia [15].

3.2. Rotation Matrices

As seen before, there are several methods to define a rotation and, thus, multiple approaches to obtain the rotation matrix $\boldsymbol{R}$ presented in equation (14). One method to effect a transformation from the axis-angle representation (ϕ along x, θ along y, and ψ along z) to their respective rotation matrices ($\boldsymbol{R}_x$, $\boldsymbol{R}_y$ and $\boldsymbol{R}_z$) specified by the Euler angles is recurring to an exponential map. Essentially, given an angle α and a unit vector $\boldsymbol{n}$ representing the unit rotation axis, the equivalent rotation matrix $\boldsymbol{R}$ can be obtained from a Taylor expansion after some algebraic manipulation as

$$\boldsymbol{R} = \boldsymbol{I} + (\sin\alpha)\boldsymbol{N} + (1 - \cos\alpha)\boldsymbol{N^2} \tag{15}$$

where $\boldsymbol{I}$ is the identity matrix and $\boldsymbol{N}$ is a skew-symmetric matrix which represents the cross-product of the unit vector $\boldsymbol{n}$. This expression is known as the *Rodrigues' rotation formula*, and, together with equation (2), is the applied solution to compute the rotation matrices in this work.

3.3. Spin Stability about the Principal Axes

For a spacecraft orbiting the Earth, according to Euler's moment equations of angular motion (9), its spin direction only changes if external moments are applied about its center of mass and perpendicular to the spin axis [1, 2]. However, it is important to notice that even in the absence of external torques, the dynamics equation still holds true. Euler's moment equations along the principal axes of inertia considering free dynamics ($\tau = 0$) are written as

$$\begin{cases} J_x\dot{\omega}_x + (J_z - J_y)\omega_y\omega_z = 0 \\ J_y\dot{\omega}_y + (J_x - J_z)\omega_z\omega_x = 0 \\ J_z\dot{\omega}_z + (J_y - J_x)\omega_x\omega_y = 0 \end{cases} \tag{16}$$

which yields, for the angular velocity rates, the following 3-state nonlinear ordinary differential equations (ODEs):

$$\begin{cases} \dot{\omega}_x = -\frac{(J_z - J_y)}{J_x}\omega_y\omega_z \\ \dot{\omega}_y = -\frac{(J_x - J_z)}{J_y}\omega_x\omega_z \\ \dot{\omega}_z = -\frac{(J_y - J_x)}{J_z}\omega_x\omega_y \end{cases} \tag{17}$$

From these homogeneous equations, the spin stabilization conditions can be analyzed at once. In this case, stability conditions for rotation about the $\boldsymbol{Z}_b$ body axis are sought. Introducing a small disturbance $\epsilon \in \mathbb{R}$ in the angular velocity so that $\omega_\ddagger = \omega_z + \epsilon$ and, consequently, $\dot{\omega}_\ddagger = \dot{\omega}_z + \dot{\epsilon} = \dot{\epsilon}$. If $\epsilon \Rightarrow 0$ then equations (16) become

$$\begin{cases} J_x\dot{\omega}_x + (J_z - J_y)\omega_y\omega_z = 0 \\ J_y\dot{\omega}_y + (J_x - J_z)\omega_z\omega_x = 0 \\ J_z\dot{\epsilon} + (J_y - J_x)\omega_x\omega_y = 0 \end{cases} \tag{18}$$

The first two equations are linear, and a second differentiation of the first using the second, yields

$$\ddot{\omega}_x + \frac{J_z - J_y}{J_y}\frac{J_z - J_x}{J_x}\omega_z^2\omega_x = 0 \tag{19}$$

and taking its Laplace transform results in the characteristic equation $\lambda(s) = s^2 - \gamma^2 = 0$, where $s = \pm\gamma$ are the roots of the characteristic equation and with $\gamma = \sqrt{(1 - J_z/J_x)(J_z/J_y - 1)\omega_z^2}$.

For at least neutral stability, all roots of $\lambda(s)$ must have a negative or no real part ($\text{Real}(s) \leq 0$). Therefore, γ needs to be an imaginary number, which means that the conditions for stability are

$$J_z > J_x, J_y \quad \text{or} \quad J_z < J_x, J_y$$

In words, if a body is spinning about its axis of minimum or maximum moment of inertia, i.e., if γ is a pure imaginary, then the angular motion is described by an harmonic oscillator, implying neutral stability along these axes. But suppose that the body spins about the axis with intermediate value of moment of inertia and so the previous condition is not satisfied. This means that

$$J_x > J_z > J_y \quad \text{or} \quad J_x < J_z < J_y$$

For this case, γ is a real number, hence one of the roots of $\lambda(s)$ is a positive real pole ($\text{Real}(s) > 0$), thus implying instability for this specific condition.

In reality, there are parasitic and non-modeled torques that dissipate energy, possibly leading to instability along the minor axis of inertia [2]. Even so, the principle of spin stability is robust if considering the principal major axis of inertia and still holds true for this situation. Therefore, the major axis solution is applied in this work.

4. Active Spin Stabilization

To develop the guidance, navigation and control (GNC) system, both a navigation filter for estimation, a guidance algorithm to determine the reference, and a control method to command the spacecraft to the desired reference must be designed. In the particular case in study, the state estimate should also include the rotation angles.

From that evaluation, the controller is designed to provide the required control torques to orient the spacecraft according to the principal major axis of inertia. This proposed solution is also known as *active spin stabilization*.

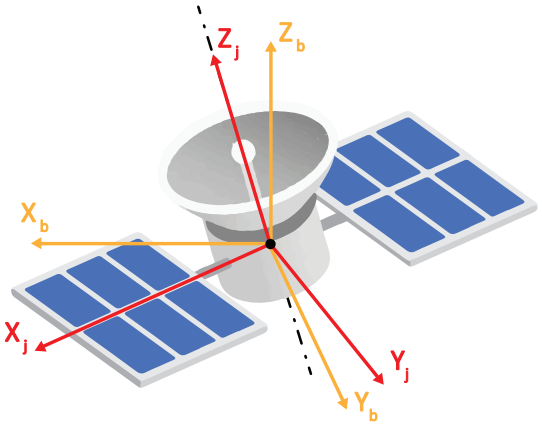

Figure 1: Spacecraft body frame $\mathcal{B}$ and principal axes of inertia reference frame $\mathcal{J}$

Figure 1 illustrates two body-centered and vehicle-carried coordinate systems - the spacecraft body frame $\mathcal{B}$ (in yellow) and the principal axes of inertia reference frame $\mathcal{J}$ (in red). Pragmatically, the active spin stabilization system is a GNC solution that takes an initial angular velocity coincident with the Z_b-axis, computes the two angles between the Z-axes, and uses them to rotate the angular velocity vector and aligned it with the Z_j-axis.

4.1. State Estimation Methods

State estimation refers to the process of finding the best estimate of the true system state from a dynamic model and a set of measured observations, both corrupted with random noise of known statistics. The variables to be estimated form the so-called *state vector*, which typically includes the attitude amongst other variables [1, 16].

A large class of estimation problems involve nonlinearities and, if a system is modeled such that it takes them into account, then the state transition function becomes nonlinear. For these situations, a nonlinear state estimator needs to be used instead of a simple Kalman filter (KF), as KFs are only defined for linear systems. In this case, the most appropriate solution is an Extended Kalman filter (EKF), which linearizes the nonlinear function around the mean of the current state estimate [16].

Table 1: Continuous-time EKF formulation

Continuous-time EKF	
Model	$\dot{\boldsymbol{x}} = \boldsymbol{f}(\boldsymbol{x}, \boldsymbol{u}, \boldsymbol{w}, t)$ $\boldsymbol{y} = \boldsymbol{h}(\boldsymbol{x}, \boldsymbol{v}, t)$
Initial condition	$\hat{\boldsymbol{x}}(0) = E[\boldsymbol{x}(0)]$ $\boldsymbol{P}(0) = E[(\boldsymbol{x}(0) - \hat{\boldsymbol{x}}(0))(\boldsymbol{x}(0) - \hat{\boldsymbol{x}}(0))^T]$
Gain	$\boldsymbol{K} = \boldsymbol{P}\boldsymbol{C}^T\boldsymbol{R}_c^{-1}$
Propagation	$\dot{\hat{\boldsymbol{x}}} = \boldsymbol{f}(\hat{\boldsymbol{x}}, \boldsymbol{u}, \boldsymbol{w}_0, t) + \boldsymbol{K}(\boldsymbol{y} - \boldsymbol{h}(\hat{\boldsymbol{x}}, \boldsymbol{v}_0, t))$ $\dot{\boldsymbol{P}} = -\boldsymbol{P}\boldsymbol{C}^T\boldsymbol{R}_c^{-1}\boldsymbol{C}\boldsymbol{P} + \boldsymbol{F}\boldsymbol{P} + \boldsymbol{P}\boldsymbol{F}^T + \boldsymbol{Q}_c$

with $\boldsymbol{w} \sim (0, \boldsymbol{Q}_k)$, $\boldsymbol{v} \sim (0, \boldsymbol{R}_k)$, $\boldsymbol{w}_0 = 0$ and $\boldsymbol{v}_0 = 0$.

Table 1 summarizes the equations of the EKF formulation. It is important to note that, contrarily to the KF for linear systems, the Extended Kalman Filter does not guarantee stability, but is still widely implemented in the scientific community, as it yields precise, accurate and stable estimates for a great majority of systems.

4.2. Control Design Methods

For active spin stabilization, there is no need to include an elaborate control law, as a simple proportional-integral controller can take the angular velocity estimate and compute the demanded control torque. However, the desired angular velocity reference can be considered more difficult to calculate, as addressing this elaborate task requires deducing an expression to relate the estimated rotation angles to the angular velocity.

Proportional-Integral (PI) control is a linear feedback control system in which the process error, i.e., the difference between the desired value and the measured value, is continuously calculated and applies a correction based on proportional and integral terms to the controlled variable. The general equation for a proportional-integral controller in a three-dimensional system ($\boldsymbol{x}, \boldsymbol{u} \in \mathbb{R}^3$) is given by

$$\boldsymbol{u}(t) = \boldsymbol{K}_p\boldsymbol{e}(t) + \boldsymbol{K}_i \int_0^t e(\tau)d\tau \tag{20}$$

where $\boldsymbol{u}(t) \in \mathbb{R}^3$ is the controller output at time t, $\boldsymbol{K}_p \in \mathbb{R}^{3\times3}$ is the proportional gain, $\boldsymbol{K}_i \in \mathbb{R}^{3\times3}$ is the integral gain, and $\boldsymbol{e}(t) \in \mathbb{R}^3$ is the instantaneous process error at time t, i.e.,

$$\boldsymbol{e}(t) = \boldsymbol{r}(t) - \boldsymbol{y}(t) \tag{21}$$

with $\boldsymbol{r}(t) \in \mathbb{R}^3$ as the reference or desired value at time t, and $\boldsymbol{y}(t) \in \mathbb{R}^3$ as the measured value at time t.

This definition can be extended for the dynamics, and used to design a torque PI controller. In this case, the external torque $\boldsymbol{\tau}$ should be defined as

$$\boldsymbol{\tau} = \boldsymbol{\omega} \times \boldsymbol{J}\hat{\boldsymbol{\omega}} + \boldsymbol{K}_p\boldsymbol{\omega}_e + \boldsymbol{K}_i \int \boldsymbol{\omega}_e \tag{22}$$

and, substituting this result on equation (9), the spacecraft attitude dynamics can be described as

$$\dot{\boldsymbol{\omega}} = -\boldsymbol{J}^{-1}(\boldsymbol{\omega} \times \boldsymbol{J}\boldsymbol{\omega}) + \boldsymbol{J}^{-1}\boldsymbol{\tau} = \boldsymbol{K}_p\boldsymbol{J}^{-1}\boldsymbol{\omega}_e + \boldsymbol{K}_i\boldsymbol{J}^{-1} \int \boldsymbol{\omega}_e \tag{23}$$

where $\boldsymbol{\omega}_e = \boldsymbol{\omega}_r - \boldsymbol{\omega}$ is the angular velocity error, with $\boldsymbol{\omega}_r$ being the angular velocity reference of the spacecraft body frame w.r.t. the inertial frame and expressed in frame $\mathcal{B}$.

The torque proportional-integral controller (22) requires an angular velocity reference $\boldsymbol{\omega}_r \in \mathbb{R}^3$ to compute the control torque. Moreover, its value should be updated throughout the simulation to keep it aligned with the major inertia axis Z_j. The expression that relates the filtered measurements and other variables to the angular velocity reference is part of the guidance algorithm. In fact, the inertia matrix $\boldsymbol{J}_{ctr}$ used for the controller can also be updated along time and included in this subsystem, but as its ultimate goal is to align the angular velocity reference with the principal major axis of inertia, the proposed applications constitute the so-called *dynamic reference guidance*.

For this problem, two different guidance solutions were studied. The first alternative takes advantage of the values provided by the navigation filter and is labeled *estimate-based guidance*. On the other hand, the second option follows a bolder approach and eliminates the need for a determination system, instead using another nonlinear control law to converge the angular velocity reference to its desired value, i.e. a vector aligned with J_z, hence being known as *control-based guidance*.

1) Estimate-Based Guidance: In this case, the state vector estimated by the navigation filter includes the rotation angles about the x-axis ($\hat{\phi} \in \mathbb{R}$) and the y-axis ($\hat{\theta} \in \mathbb{R}$) for the frame transformation of $\mathcal{B}$ to $\mathcal{J}$, and those values can be used to update the angular velocity reference.

Therefore, using the rotation matrix product (2), the angular velocity reference $\boldsymbol{\omega}_r$ can be updated according to

$$\boldsymbol{\omega}_r = \boldsymbol{R}(\hat{\phi}, \hat{\theta})\boldsymbol{\omega}_{r_0} \tag{24}$$

where $\boldsymbol{\omega}_{r_0}$ is the initially desired angular velocity of the spacecraft body frame w.r.t. the inertial reference frame and represented in the body coordinate system.

Furthermore, the rotation matrix $\boldsymbol{R}(\hat{\phi}, \hat{\theta})$, together with Sylvester's law of inertia (14), can also be used to update the diagonal inertia tensor $\boldsymbol{J}_{ctr}$, as given by

$$\boldsymbol{J}_{ctr} = \boldsymbol{R}(\hat{\phi}, \hat{\theta})\boldsymbol{J}_{ctr_0}\boldsymbol{R}(\hat{\phi}, \hat{\theta})^T \tag{25}$$

where $\boldsymbol{J}_{ctr_0}$ is the initial estimate for the diagonal inertia matrix, which is the main diagonal of the inertia tensor.

2) Control-Based Guidance: Another way to address the problem at hand is to find a relation between the angular velocity reference $\boldsymbol{\omega}_r$ and the external torque $\boldsymbol{\tau}$, and thus introduce a novel guidance law that updates the angular velocity reference according to the current torque values. The intuition used to define this method is the fact that there is necessarily a commanded torque to maintain the satellite spinning around an unstable axis, i.e., when $\boldsymbol{\omega}_r$ is unaligned with the principal major axis of inertia. Additionally, this reasoning suggests that torque values are related to the difference between the angular velocity direction and the major inertia axis orientation.

Ideally, the stationary case should be a free dynamics situation as well, because in case the angular velocity reference has been promptly corrected and aligned with the principal major axis of inertia, then these directions overlap and there is no difference between them, meaning that the external torque should also converge to zero. In other words, if the dynamics equation (9) tends to the appropriate $\boldsymbol{\omega}_r$, it can be reduced to $\dot{\boldsymbol{\omega}}_r = 0 \iff \boldsymbol{\omega}_r \times \boldsymbol{J}_{ctr}\boldsymbol{\omega}_r = 0$.

Therefore, the first step in this strategy is to solve the dynamics equation for the angular velocity reference $\boldsymbol{\omega}_r$, in order to obtain a result suitable for a controller design that leads the system to a torque-less dynamics state.

One suitable obtained result for the equation is

$$\begin{aligned} \omega_{r_1} &= \frac{1}{(J_1 - J_3)} \cdot \frac{\tau_2}{z} \\ \omega_{r_2} &= -\frac{1}{(J_2 - J_3)} \cdot \frac{\tau_1}{z} \quad , \quad J_1 \neq J_3, J_2 \neq J_3, \tau_3 = 0 \\ \omega_{r_3} &= z \qquad\qquad\qquad , \quad z \in \mathbb{R} \end{aligned} \tag{26}$$

This solution provides an elegant, simple and intuitive relation between the angular velocity reference and the external torque. Thereafter, in compliance with the necessary conditions and keeping $\omega_{r_3} = z$ constant, the angular velocity references ω_{r_1} and ω_{r_2} should evolve in the direction that draws them closer to the obtained solutions, i.e., according to the following equations:

$$\begin{cases} \delta\dot{\omega}_{r_1} = -K_1 C_1 \tau_2 & , \quad C_1 = \frac{1}{(J_1 - J_3)z} \\ \delta\dot{\omega}_{r_2} = -K_2 C_2 \tau_1 & , \quad C_2 = -\frac{1}{(J_2 - J_3)z} \end{cases} \tag{27}$$

where $K_1, K_2 \in \mathbb{R}$ are the proportional gains for the variations of the angular velocity references $\delta\omega_{r_1}$ and $\delta\omega_{r_2}$.

Therefore, the dynamic angular velocity reference $\boldsymbol{\omega}_r$ is updated by

$$\boldsymbol{\omega}_r = \boldsymbol{\omega}_{r_0} + \delta\boldsymbol{\omega}_r \quad \text{with} \quad \delta\boldsymbol{\omega}_r = \begin{bmatrix} \delta\omega_{r_1} & \delta\omega_{r_2} & 0 \end{bmatrix}^T \tag{28}$$

where $\boldsymbol{\omega}_{r_0}$ is the initially desired angular velocity of the spacecraft body frame w.r.t. the inertial reference frame and represented in the body coordinate system.

After a certain time, the angular velocity reference converges to the correct value and maintains a stationary behavior, which is represented from now on as $\boldsymbol{\omega}_s \in \mathbb{R}^3$. From the initial angular velocity reference $\boldsymbol{\omega}_{r_0}$ and projecting a new stationary angular velocity vector in the $y0z$-plane ($\boldsymbol{\omega}_{s_x} \in \mathbb{R}^3$) and in the $x0z$-plane ($\boldsymbol{\omega}_{s_y} \in \mathbb{R}^3$), it becomes possible to compute the rotation angles ϕ_{ctr} and θ_{ctr} using the arc tangent trigonometric notion. Furthermore, these angles can be used to compute the rotation matrix $\boldsymbol{R}(\phi_{ctr}, \theta_{ctr})$ and update the diagonal control inertia matrix $\boldsymbol{J}_{ctr}$, as illustrated in equation (25) for the estimate-based guidance.

However, this approach is incomplete as it ignores that, since $\delta\omega_{r_3} = 0$ and, consequently, $\boldsymbol{\omega}_s(3) = \boldsymbol{\omega}_{r_0}(3)$ in the spacecraft body frame, it can be mathematically confirmed that $||\boldsymbol{\omega}_s|| > ||\boldsymbol{\omega}_{r_0}||$, which implies that, regardless of the alignment with the major inertia axis, the satellite is spinning at a faster rate than intended.

To amend the control-based guidance algorithm, an equation for $\delta\omega_{r_3}$ must be added to guarantee that the norm of both the initial and the stationary angular velocity references have the same value. This condition can be ensured by the following expression:

$$\delta\omega_{r_3} = \sqrt{||\boldsymbol{\omega}_{r_0}||^2 - (\omega_{s_1}^2 + \omega_{s_2}^2)} - \omega_{r_{0_3}} \tag{29}$$

Finally, the dynamic reference guidance equation (28) is revised and the variation of the angular velocity reference is redefined to $\delta\boldsymbol{\omega}_r = \begin{bmatrix} \delta\omega_{r_1} & \delta\omega_{r_2} & \delta\omega_{r_3} \end{bmatrix}^T$.

At last, the Lyapunov criteria for a nonlinear system can be used to determine the stability of the designed PI controller. According to Lyapunov's global asymptotic stability (GAS) theorem, if there exists a scalar function $\boldsymbol{V}(x) : \mathbb{R}^n \to \mathbb{R}$, with continuous first order derivatives such that *1)* $\boldsymbol{V}(x)$ is globally positive definite, *2)* $\dot{\boldsymbol{V}}(x)$ is globally negative definite, and *3)* $\boldsymbol{V}(x)$ is radially unbounded, then the equilibrium point at the origin is globally asymptotically stable.

The selected Lyapunov candidate function is given by

$$\boldsymbol{V}(\boldsymbol{\omega}_e) = \frac{1}{2}\boldsymbol{\omega}_e^T \boldsymbol{J}\boldsymbol{\omega}_e + \frac{1}{2}\left(\int \boldsymbol{\omega}_e\right)^T \boldsymbol{K}_i \int \omega_e \tag{30}$$

which is a typical quadratic form polynomial, thus, as the Sylvester's criterion holds for the positive semi-definite inertia tensor $\boldsymbol{J}$ and for $\boldsymbol{K}_i > 0$, it guarantees that $\boldsymbol{V}(\boldsymbol{\omega}_e)$ is globally positive definite.

From equation (23), the Lyapunov candidate function time-derivative $\dot{\boldsymbol{V}}(\boldsymbol{\omega}_e)$ can be calculated as

$$\dot{\boldsymbol{V}}(\boldsymbol{\omega}_e) = \frac{\partial \boldsymbol{V}}{\partial \boldsymbol{\omega}_e} \cdot \frac{\partial \boldsymbol{\omega}_e}{\partial t} = -\boldsymbol{K}_p \boldsymbol{\omega}_e^2 \leq 0 \quad , \quad \text{if} \quad \boldsymbol{K}_p > 0 \tag{31}$$

where the angular velocity error time-derivative $\dot{\boldsymbol{\omega}}_e$ is defined by

$$\dot{\boldsymbol{\omega}}_e = \dot{\boldsymbol{\omega}}_r - \dot{\hat{\boldsymbol{\omega}}} = -\dot{\hat{\boldsymbol{\omega}}} \tag{32}$$

and with the torque control law being deemed sufficiently fast to consider the angular velocity reference constant and, consequently, its derivative null.

Hence, as $\boldsymbol{K}_p > 0$ and $\dot{\boldsymbol{V}}(\boldsymbol{\omega}_e) = 0$ iff $\boldsymbol{\omega}_e = 0$, then $\dot{\boldsymbol{V}}(\boldsymbol{\omega}_e)$ is globally negative definite. Therefore, since the Lyapunov function (30) is also radially unbounded, it is possible to conclude that the PI controller is globally asymptotically stable at the zero-error equilibrium point.

5. Implementation

To determine the feasibility and viability of active spin stabilization, the development of a simulation environment is a practical and realistic approach to implement the presented solutions. This model comprises two main blocks - the Spacecraft Plant and the Control System.

5.1. Spacecraft Plant

To recreate the space environment around a satellite, the Spacecraft Plant model is composed of an orbital dynamics model to define the satellite's position in a circular orbit around the Earth, a disturbances model that simulates the effects of external perturbances torques on the spacecraft, kinematics and dynamics models to propagate the satellite's attitude, and sensors and actuators models that reproduce their characteristic measurement outputs and control inputs, respectively.

It should be noted that the remaining disturbances torque $\boldsymbol{\tau}_r \in \mathbb{R}^3$ is modeled as a zero-mean Gaussian distribution computed from a small percentage of the gravity-gradient torque norm, the quaternion kinematics have Baumgarte stabilization [17] introduced in their equation, and the actuators include an estimation of the expelled propellant mass variation $\Delta M \in \mathbb{R}$ based on the control torque, calculated by

$$\Delta M = \int \frac{\sum_{n=1}^{3} |\tau_n|}{g_0 I_{sp} d_{CM}} \tag{33}$$

5.2. Control System

On the other hand, the Control System is responsible for applying the active spin stabilization described in Section 4, namely, the navigation filter, both guidance algorithms and the control law. Its objective is to use the measurements provided by the rate gyros to determine the required torque that the thrusters must exert to achieve the desired spacecraft angular velocity.

5.3. Simulation Parameters

For this study, the satellite model and its properties are considered to be constant. Thus, except for the real inertia matrix $\boldsymbol{J}$ in the body reference frame, the Spacecraft Plant is the same at all times. In fact, many parameters never change throughout the entire implementation and testing phase. Therefore, to provide a simple process to consult their values, every single one is listed in Table 2.

Table 2: Simulation parameters

Parameter	Notation	Value
Satellite Mass	m_{sat}	$400\,\text{kg}$
Moments of Inertia	J_{ii}	$[360 \quad 280 \quad 500]\,\text{kg}\cdot\text{m}^2$
Products of Inertia	J_{ij}	$[30 \quad -40 \quad 35]\,\text{kg}\cdot\text{m}^2$
Circular Orbit Reference Altitude	h	$600\,\text{km}$
Orbit Inclination	i	$100\,\text{deg}$
Gravity-Gradient Torque Std. Dev.	σ_{gg}	$5.605 \times 10^{-4}\,\text{N}\cdot\text{m}$
Remaining Disturbances Torque Std. Dev.	σ_r	$5.605 \times 10^{-5}\,\text{N}\cdot\text{m}$
Rate Gyroscopes Sample Frequency	f_ω	$100\,\text{Hz}$
Angular Velocity Noise Std. Dev.	σ_ω	$1 \times 10^{-6}\,\text{rad/s}$
Thrusters' Specific Impulse	I_{sp}	$290\,\text{s}$
Maximum control torque	τ_{max}	$20\,\text{N}\cdot\text{m}$
Distance from the Actuators to the CoM	d_{CM}	$\sqrt{3}\,\text{m}$
Angular Velocity Process Noise	$\boldsymbol{Q}_c^\omega$	$1 \times 10^{-2} \cdot \boldsymbol{I}_3$
Rotation Angles Process Noise	$\boldsymbol{Q}_c^\alpha$	$1 \times 10^{-2} \cdot \boldsymbol{I}_2$
Principal Axis of Inertia Process Noise	$\boldsymbol{Q}_c^J$	$1 \times 10^{0} \cdot \boldsymbol{I}_3$
Measurement Noise	$\boldsymbol{R}_c$	$1 \times 10^{-3} \cdot \boldsymbol{I}_3$
Angular Velocity Initial Covariance	$\boldsymbol{P}_0^\omega$	$1 \times 10^{-3} \cdot \boldsymbol{I}_3$
Rotation Angles Initial Covariance	$\boldsymbol{P}_0^\alpha$	$1 \times 10^{0} \cdot \boldsymbol{I}_2$
Principal Axis of Inertia Initial Covariance	$\boldsymbol{P}_0^J$	$1 \times 10^{3} \cdot \boldsymbol{I}_3$
Proportional Gain for $\delta\omega_{r_1}$	K_1	1×10^{-2}
Proportional Gain for $\delta\omega_{r_2}$	K_2	1×10^{-2}
Proportional Gain for Torque Control	$\boldsymbol{K}_p$	100
Integral Gain for Torque Control	$\boldsymbol{K}_i$	2

6. Simulation Results

The final goal of this study consists in taking advantage of the simulation environment and evaluate the sensitivity and robustness of the active spin stabilization control system. For that purpose, a Monte Carlo analysis is carried out with all simulations including noise and disturbances.

6.1. Setup

For the initial parameters, the real inertia matrix $\boldsymbol{J}$ is obtained from Sylvester's law of inertia (14), where the principal moments of inertia $\boldsymbol{\Lambda}$ are constant, but the rotation angles that compose the rotation matrix $\boldsymbol{R}$ (ϕ and θ) can range from -30 to $30\,\text{deg}$, in order to collect a broad set of different orientations for the major axis of inertia.

Furthermore, matrix $\boldsymbol{J}_{ctr_0}$ is also defined by the principal moments of inertia, albeit with the introduction of an independent $\pm 10\%$ initial error to replicate the control inertia matrix uncertainty. On top of that, both rotation angles initial estimates ϕ_0 and θ_0 are null, as the spacecraft body frame is initially believed to be aligned with the principal axes of inertia, and the initial angular velocity estimate $\boldsymbol{\omega}_0$ is arbitrary. All the initial conditions for the parameters and reference values are presented in Table 3.

Table 3: Initial conditions for the Monte Carlo analysis

Variable	Notation	Value
Simulation Time	t	$3000\,\text{s}$
Sample Frequency	f_S	$20\,\text{Hz}$
Principal Moments of Inertia	$\boldsymbol{\Lambda}$	$\text{diag}([360 \quad 280 \quad 500])\,\text{kg}\cdot\text{m}^2$
Rotation Angle in x-Axis	ϕ	$\pm\,[0; 30]\,\text{deg}$
Rotation Angle in y-Axis	θ	$\pm\,[0; 30]\,\text{deg}$
Ang. Vel. Reference	$\boldsymbol{\omega}_{r_0}$	$[0 \quad 0 \quad 10]\,\text{deg/s}$
Ang. Vel. Variance Reference	$\delta\boldsymbol{\omega}_{r_0}$	$[0 \quad 0 \quad 0]\,\text{deg/s}$
Angular Velocity	$\boldsymbol{\omega}_0$	$\pm\,[[0;1]\,[0;1]\,[0;1]]\,\text{deg/s}$
Rotation Angle in x-Axis	ϕ_0	$0\,\text{deg}$
Rotation Angle in y-Axis	θ_0	$0\,\text{deg}$
Control Inertia Matrix	$\boldsymbol{J}_{ctr_0}$	$\pm\,[0;10]\,[0;10]\,[0;10]]\% \cdot \boldsymbol{\Lambda}\,\text{kg}\cdot\text{m}^2$

6.2. Results

In order to develop a clear and simple strategy to validate the Control System's reliability, the 100 different iterations of the Monte Carlo analysis are evaluated according to three performance criteria.

Each criterion has been determined to address the most important factors to assure that the solution is achieving the desired results. In specific, the performance criteria are defined by the root-mean-square error (RMSE) for the:

1. Angle between Z_j and the angular velocity $\alpha_{J_3\omega}$
2. Vector norm of the angular velocity error $||\boldsymbol{\omega}_e||$
3. Vector norm of the external torque $||\boldsymbol{\tau}||$

To decide whether the performance criteria are fulfilled, distinct thresholds have been defined for each one. These limit values are selected according to the expected results from several previous tests. In case the three performance criteria converge to a steady-state value under the defined thresholds, without ever breaching the convergence envelope, then the Control System can be deemed as stable and robust according to the Monte Carlo analysis.

1) Estimate-Based Guidance: For this method, all the performance criteria intersect the threshold and permanently stay inside the convergence envelope in about 500 s. There are still some accumulated oscillations for the lower orders of magnitude due to the noise and external disturbances affecting the system, but these do not compromise the convergence objective, as seen in Figures 2, 3 and 4.

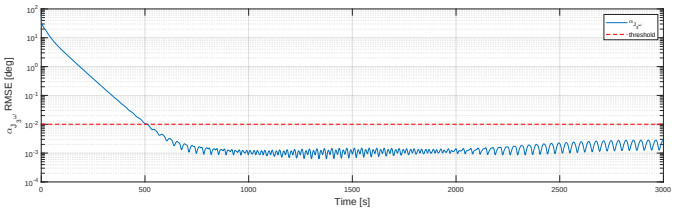

Figure 2: Performance criterion #1 - $\alpha_{J_3\omega}$

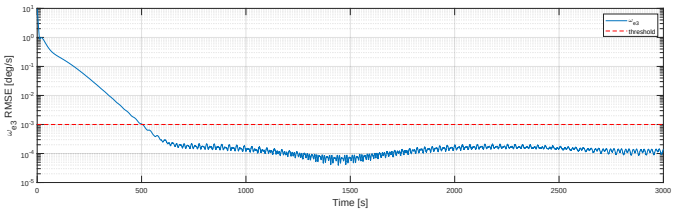

Figure 3: Performance criterion #2 - $||\boldsymbol{\omega}_e||$

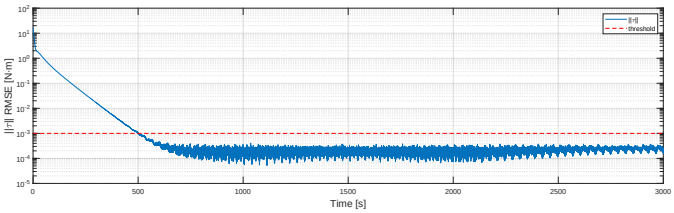

Figure 4: Performance criterion #3 - $||\boldsymbol{\tau}||$

At last, the mean fuel consumption and the mean fuel saving estimates are included in this analysis to conclude that the Control System steadily reduces the propellant usage of the spacecraft. Indeed, Figure 5 illustrates that the mean total fuel consumption is estimated to be 0.0504 kg and the fuel saving estimate is 96.3859%, when compared to 1.3949 kg spent in a no-guidance simulation.

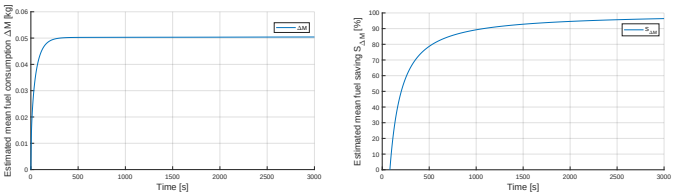

(a) Mean fuel consumption $\overline{\Delta M}$ (b) Mean fuel saving $\overline{S_{\Delta M}}$

Figure 5: Fuel consumption (5(a)) and fuel saving (5(b))

2) Control-Based Guidance: Similarly, the control-based solution also complies with the three performance criteria, but it takes more time to enter the convergence envelope and settle to a constant value. In fact, the average threshold cross-time for this method is approximately double of the estimate-based one, i.e., over around 1000 s.

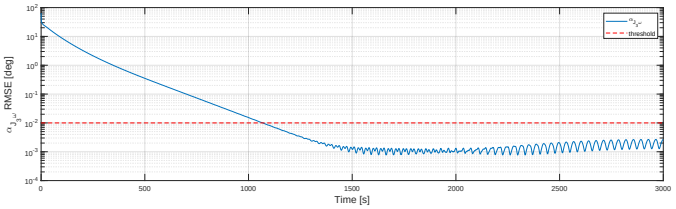

Figure 6: Performance criterion #1 - $\alpha_{J_3\omega}$

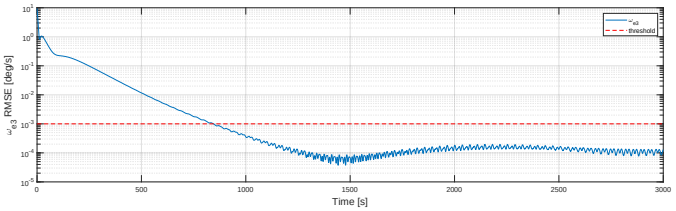

Figure 7: Performance criterion #2 - $||\boldsymbol{\omega}_e||$

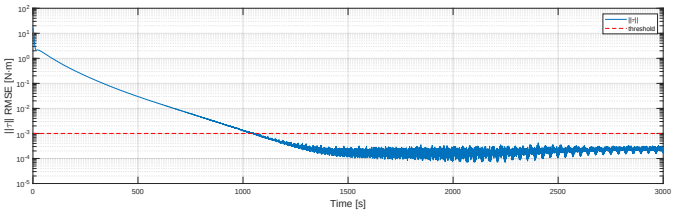

Figure 8: Performance criterion #3 - $||\boldsymbol{\tau}||$

The increased time to reach the desired steady-state evolution translates to an increased fuel consumption. Indeed, the total mean propellant expelled mass estimate is 0.0782 kg, thus resulting in an estimated reduction of 94.3933% in energy usage for the total simulation time.

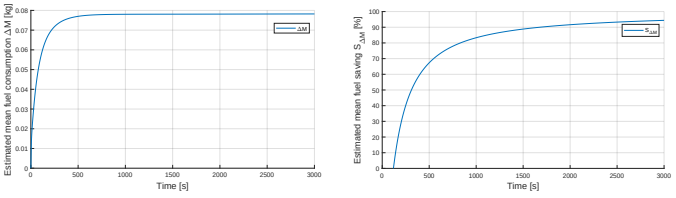

(a) Mean fuel consumption $\overline{\Delta M}$ (b) Mean fuel saving $\overline{S_{\Delta M}}$

Figure 9: Fuel consumption (9(a)) and fuel saving (9(b))

To sum up, the Monte Carlo analysis provides strong evidence to safely conclude that both guidance methods lead to major improvements in power efficiency for a great variety of initial conditions and parameters. In addition,

the introduction of an EKF seems to generally drive the spacecraft to converge twice as fast to the performance criteria, thus reducing propellant usage and increasing the space mission duration. As a final analysis comparison, the mean RMSE values of the three performance criteria are evaluated for the last 1500 s of simulation time, as all variables exhibit a steady-state evolution in that time interval. Alongside the mean fuel consumption and saving, these mean values are included in Table 4.

Table 4: Guidance comparison for Monte Carlo analysis

Guidance Method	Performance Criteria			Fuel	
	$\|\|\bar{\omega_e}\|\|$ [deg/s]	$\|\bar{\alpha_{J_3\omega}}\|$ [deg]	$\|\|\bar{\tau}\|\|$ [N·m]	ΔM [kg]	$S_{\Delta M}$ [%]
No Guidance	8.9489×10^{-5}	15.3385	1.6191	1.3949	———
Estimate-Based	1.3561×10^{-4}	1.5054×10^{-3}	1.9518×10^{-4}	0.0504	96.3859
Control-Based	1.2627×10^{-4}	1.4030×10^{-3}	1.8345×10^{-4}	0.0782	94.3933

From the listed criteria, the estimate-based guidance can be considered the best method for the tested parameters and gains, due to its reduced fuel usage and a non-significant performance difference w.r.t. the other solution. Nevertheless, the computational load imposed by the EKF is a considerable drawback. In fact, as the control-based guidance has fewer mathematical operations than the estimate-based solution, the former method can run the simulation 16.36× faster than the real time, while the latter can only simulate up to 4.36× the real time.

7. Conclusions

In this document, the main objective was to study, design, implement and test an active spin stabilization system, able to align the satellite's spinning axis to the principal major axis of inertia, and therefore reduce the fuel consumption and increase the space mission time. The obtained results serve as evidence that both guidance methods are able to considerably reduce fuel consumption, even for different initial conditions and parameters.

The estimate-based guidance can be considered the preferred method, due to its reduced total propellant usage and no significant performance difference from the control-based guidance. Nevertheless, the former solution extended time to simulate must be looked upon as the computational efficiency is an important factor when deciding which guidance algorithm to implement in the spacecraft.

As a concluding remark, it should be noted that the obtained results are dependent on the parameters and gains previously defined and listed in Table 2, implying that other values could generate slightly different outcomes. In fact, after a more exhaustive analysis to fine-tune the guidance proportional gains, it should be possible to decrease the settling time for the control-based method variables.

Further improvements include the possibility of testing the simulation environment for a non-constant inertia tensor, i.e., to include small variations in the inertia matrix and evaluate the Control System ability to adapt and still converge for this dynamic condition. In addition, actuators have physical limitations, determining that thrusters must be turned on for a minimum time, which could become an issue for small commanded torques. Therefore, a minimum limit value could be defined in the actuation system and, thus, depict more realistic actuators models.

Another important avenue of future work is the deduction of a new Lyapunov function that includes the dynamic angular velocity reference, in order to theoretically assess the Control System stability. Finally, the spinning axis orientation w.r.t. the inertial frame can be an important factor to control and, as such, one last step is to upgrade the current state vector to also include the attitude, in order to take advantage of the fuel saving provided by this GNC solution and replace the original system.

Acknowledgements

The author would like to thank Professor David Cabecinhas and Doctor Pedro Lourenço, for their helpful insight and expertise, which were crucial for this research study.

References

[1] F. L. Markley and J. L. Crassidis. *Fundamentals of Spacecraft Attitude Determination and Control*. Springer, 1^{st} edition, 2014. ISBN:9781493908011.

[2] M. J. Sidi. *Spacecraft Dynamics & Control: A Practical Engineering Approach*. Cambridge University Press, 1^{st} edition, 1997. ISBN:9780511815652.

[3] J. W. Wertz. *Spacecraft Attitude Determination and Control*. Astrophysics and Space Science Library, 1^{st} edition, 1978. ISBN:9789027712042.

[4] Y. Yang. *Spacecraft Modelling, Attitude Determination, and Control: Quaternion-Based Approach*. CRC Press, 1^{st} edition, 2019. ISBN:9781138331501.

[5] J. L. Crassidis, F. L. Markley, and Y. Cheng. Survey of Nonlinear Attitude Estimation Methods. *Journal of Guidance, Control, and Dynamics, 30(1)*, 2007.

[6] R. E. Roberson. Two Decades of Spacecraft Attitude Control. *Journal of Guidance, Control, and Dynamics, 2(1)*, 1979.

[7] L. Euler. *Theoria motus corporum solidorum seu rigidorum*. Novi Commentarii academiae scientiarum Petropolitanae, 1^{st} edition, 1765.

[8] A. Y. Lee and J. A. Wertz. In-Flight Estimation of the Cassini Spacecraft's Inertia Tensor. *Journal of Spacecraft and Rockets, 39(1)*, 2002.

[9] J. A. Keim, A. B. Aqikmese, and J. F. Shields. Spacecraft Inertia Estimation Via Constrained Least Squares. *2006 IEEE Aerospace Conference*, 2006.

[10] M. C. Norman and M. A. Peck. In-Orbit Estimation of Inertia and Momentum-Actuator Alignement Parameters. *Journal of Guidance, Control, and Dynamics, 34(6)*, 2011.

[11] R. Linares, F. A. Leve, M. K. Jah, and J. L. Crassidis. Space Object Mass-Specific Inertia Matrix Estimation from Photometric Data. *Advances in the Astronautical Sciences*, 2012.

[12] C. Nainer, H. Garnier, M. Gilson, H. Evain, and C. Pittet. In-Flight Inertia Matrix Estimation of a Gyroless Satellite. *2019 Conference in Guidance, Navigation & Control in Aerospace (EuroGNC19)*, 2019.

[13] B. Wie. *Space Vehicle Dynamics and Control*. American Institute of Aeronautics and Astronautics, 2^{nd} edition, 2008. ISBN:9781563479533.

[14] P. C. Hughes. *Spacecraft Attitude Dynamics*. Courier Corporation, 1^{st} edition, 2004. ISBN:9780486140131.

[15] J. J. Sylvester. A demonstration of the theorem that every homogeneous quadratic polynomial is reducible by real orthogonal substitutions to the form of a sum of positive and negative squares. *Philosophical Magazine and Journal of Science, 4(23)*, 1852.

[16] D. Simon. *Optimal State Estimation: Kalman, H_∞, and Nonlinear Approaches*. John Wiley & Sons, 1^{st} edition, 2006. ISBN:9780471708582.

[17] S. Gros, M. Zanon, and M. Diehl. Baumgarte stabilisation over the SO(3) rotation group for control. *54th IEEE Conference on Decision and Control (CDC)*, 2015.